Continental Shelf Research 158 (2018) 33–44

Contents lists available at ScienceDirect

Continental Shelf Research

journal homepage: www.elsevier.com/locate/csr

Research papers

Estuarine development and early Holocene transgression across an aeolianite substrate, Caesarea, central Israel

John A. Goff [a,*], James A. Austin Jr.[a], Beverly N. Goodman-Tchernov[b]

[a] Institute for Geophysics, Jackson School of Geosciences, University of Texas at Austin, United States
[b] Leon Charney School of Marine Sciences, Department of Marine Geosciences, University of Haifa, Israel

ARTICLE INFO

Keywords:
Sea-level
Transgression
Regression
Marine sand
Estuary
Climate

ABSTRACT

Estuaries are important features on the coastal landscape due to their potential for rich, diverse, and abundant resources. The modern coast of the southeast Mediterranean is largely devoid of estuaries except in rare circumstances where ample sands are delivered to the shore, such as east of the Nile Delta. Whether or not today's condition is reflective of that present during lower sea-levels is greatly speculative in part due to a dearth of high-resolution sub-surface mapping in the shallower (< 45 m) continental shelf. We report here on a multibeam bathymetry and near-surface seismic stratigraphy survey offshore of Caesarea, along the central Israeli coast; within which we find evidence of preserved estuarine sediments in water depths ~45–10 mbsl, both within paleo-channels of the Crocodile and Hadera rivers, and more broadly across the shelf. These water depths correspond to early Holocene dates (~10.5–7.5 ka) which, based on global sea-level curves, was a period of rapid (~1–1.7 cm/yr) sea-level rise. Now-submerged aeolianite ridges (locally referred to as 'kurkar'), cemented aeolian deposits formed during pre-Last-Glacial-Maximum (LGM) seaward advance (regression) of the coastline, likely provided some offshore barrier for estuarine development. These were insufficient, however, to account for all the estuarine deposition interpreted, leading us to hypothesize that sand-constructed barrier islands were also present as sea-level rose during the Holocene. This supply of sand, clearly greater than what is evident today, could have originated from sea-level rise phase eroding Nile Delta sediments transported northward by littoral currents, or from increased output from local rivers during wetter climatic conditions. We also observe a transition from linear, shore-parallel aeolianite ridge morphology features on land and in shallow water, to nested, arcuate features below ~30 mbsl. Whereas the linear ridges are thought to be coastal foredune remnants abandoned by the retreating shoreline, the arcuate forms resemble fossil parabolic (blowout) dunes. Based on the recent initiation of parabolic dunes on Cape Cod following anthropogenic denudation of forests there, we suggest that climate aridification approaching the LGM could have denuded vegetation along the Israeli coast, enabling parabolic dune formation landward of the coastal foredunes which were later preserved via cementation. Understanding the past landscape of the offshore allows for better reconstruction of dune formation, river channel presence, and identification of habitats conducive to prehistoric human exploitation and settlement.

1. Introduction

The coastal plains of the modern southeastern Mediterranean Sea are largely devoid of beach barrier-protected estuarine systems. From the Suez Canal to the Lebanese highlands, only one significant modern estuary exists, located at Bardawil Lake (Fig. 1), a ~75 km-long lagoon east of the Nile River Delta formed by barriers spits/islands sourced from Nile sediments (Levy, 1974). Barrier-protected estuaries are common elsewhere in Mediterranean coastal plain settings where high sediment supply exists, such as southern France in association with the Rhone River (Vella et al., 2005), and the northern Adriatic associated with the Po River (Stefani and Vincenzi, 2005). In contrast, the observed scarcity of barrier/estuarine systems along southeastern Mediterranean coastal plains is an indication of the lack of modern sand inputs to the coast (e.g., FitzGerald et al., 2008), aside from the Nile River, in this generally arid region. However, a recent stratigraphic study by Shtienberg et al. (2016) offshore of Israel's Hadera power plant, ~10 km from the Hadera River outlet (Fig. 1), provides evidence that estuarine development occurred along the Israeli coast during the early Holocene. Throughout much of the Shtienberg et al. (2016) survey region, which spans ~1.5 km along the coastline to water depths of ~26 mbsl, they found seismically laminated, muddy deposits up to

* Corresponding author at: Institute for Geophysics, Jackson School of Geosciences, University of Texas at Austin, United States.
E-mail address: goff@ig.utexas.edu (J.A. Goff).

https://doi.org/10.1016/j.csr.2018.03.001
Received 20 September 2017; Received in revised form 24 January 2018; Accepted 1 March 2018
Available online 06 March 2018
0278-4343/

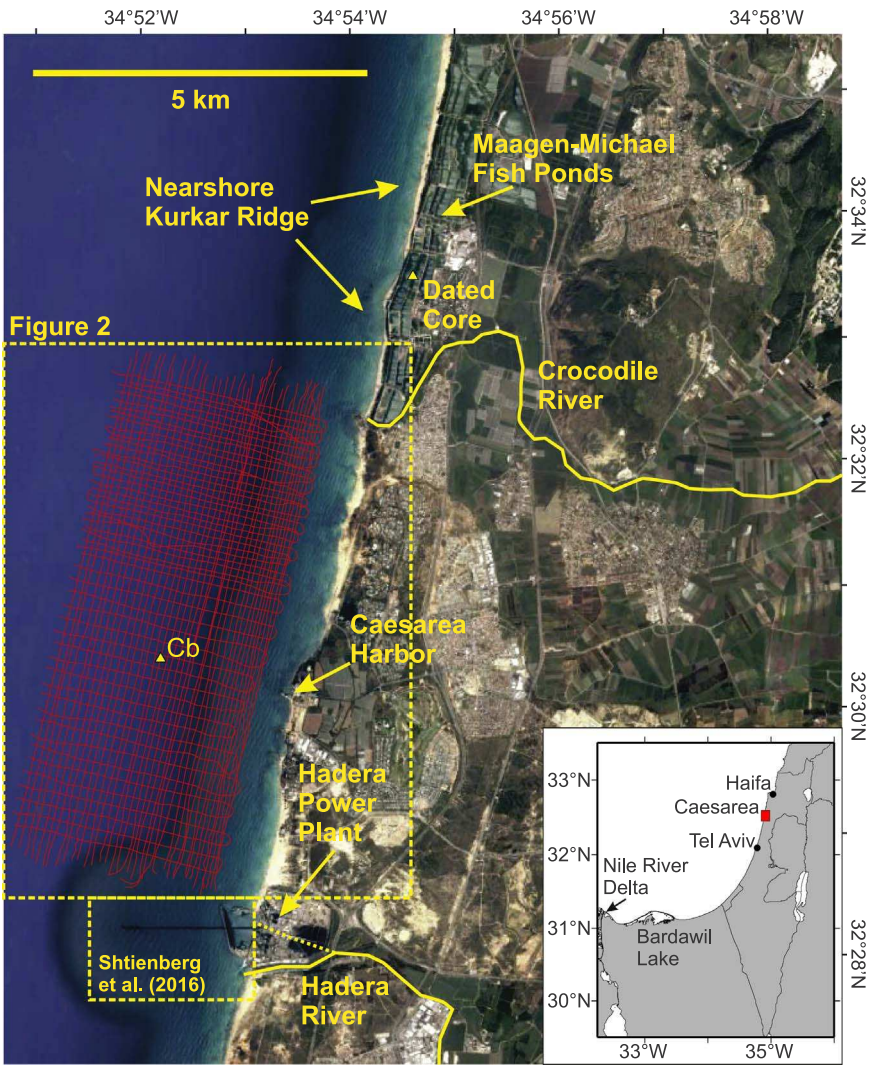

Fig. 1. Modern physiography in the vicinity of Caesarea, Israel. Image from Google Earth. Dashed portion of Hadera River indicates course prior to building of the power plant in 1982 (Shtienberg et al., 2016). Inset shows location (red box) along the Israeli coast. Red lines are chirp and multibeam track lines for the 2015 survey, which builds upon the imaging reported in Goodman-Tchernov and Austin (2015). Results from the "Dated Core", taken within the Maagden-Michael fish ponds, was presented in Cohen-Seffer et al. (2005) and further discussed in Sivan et al. (2011) and Shtienberg et al. (2016). "Cb" identifies the offshore location of a core with age dates discussed in Stienberg et al. (2016) that they stratigraphically correlate to the onshore core.

7 m thick, preserved beneath an interpreted transgressive marine sand sheet. If these sediments indicate an estuarine environment at lower sea levels, as their presence suggests elsewhere, this would indicate that coastal conditions offshore of Israel were different in the past than at present, possibly relating both to temporally varying climate and riverine sedimentary inputs.

Holocene coastal evolution along the northern Israeli coast has been influenced by prominent, lithified aeolian deposits (locally referred to as "kurkar") formed in the late Pleistocene; these are present today both on land (Sivan and Porat, 2004) and offshore at various water depths (Zviely et al., 2006; Boyce et al., 2009; Schattner et al., 2010; Goodman-Tchernov and Austin, 2015). Because these hard-rock ridges are in places now exposed at the seafloor along the innermost shelf (Sade et al., 2006), they would have had a significant role in the changing geomorphology of the coastline, post-LGM. For example, these prominent features could have formed embayments that allowed for estuarine sedimentation during the Holocene transgression.

In this paper, we seek to understand the evolution of the early Holocene/post-LGM coastline along the central Israeli coast, and in particular to investigate the possibility of associated estuarine development. We employ a concurrent chirp high-resolution seismic reflection and multibeam bathymetry survey (Figs. 1, 2) with coverage that extends ~8 km alongshore, covers water depths of ~45 mbsl to ~10 mbsl, and abuts the northern edge of the Shtienberg et al. (2016) survey area (Figs. 1, 2). Our survey, acquired in 2015, is centered approximately offshore of the harbor mouth of the ancient port city of Caesarea, between the Crocodile (or "Taninim" in Hebrew) and Hadera River outlets (Fig. 1).

1.1. Site selection: evidence for human occupation

The study site was selected because it fulfilled a range of baseline criteria that were presumed to improve the feasibility of locating and identifying complex submerged features, as well as associating them with past human occupation. Today, the modern coastline includes the ancient harbor city of Caesarea, originally constructed by King Herod between 25 and 9/10 BCE (Holum and Raban, 1996). Pre-Caesarea settlement includes a Greek colony (Raban, 2009). Documented prehistoric remains at the site itself are sparse, but nearby to the north, submerged prehistoric sites are documented offshore at Neve Yam, Atlit and Kfar Galim (Galili et al., 1993; Gopher, 1993; Raban, 1983; Raban and Galili, 1985). Most of these sites were discovered following winter storms that exposed artifacts at the seafloor. Caesarea is closer to the primary sediment source of the area, the Nile River (Zviely et al., 2007). Therefore, the possibility of more deeply buried submerged prehistoric sites exists offshore of the modern remains of Caesarea. Already, some suspected features have been identified meriting further investigation, such as a circular feature identified using magnetometry of the seafloor offshore of Caesarea in 2000 (Boyce et al., 2004). The uppermost portion of this feature was exposed briefly as a result of a significant storm in 2010, but was quickly reburied under sand. Recent studies suggest that one or more tsunami may have contributed to eventual destruction

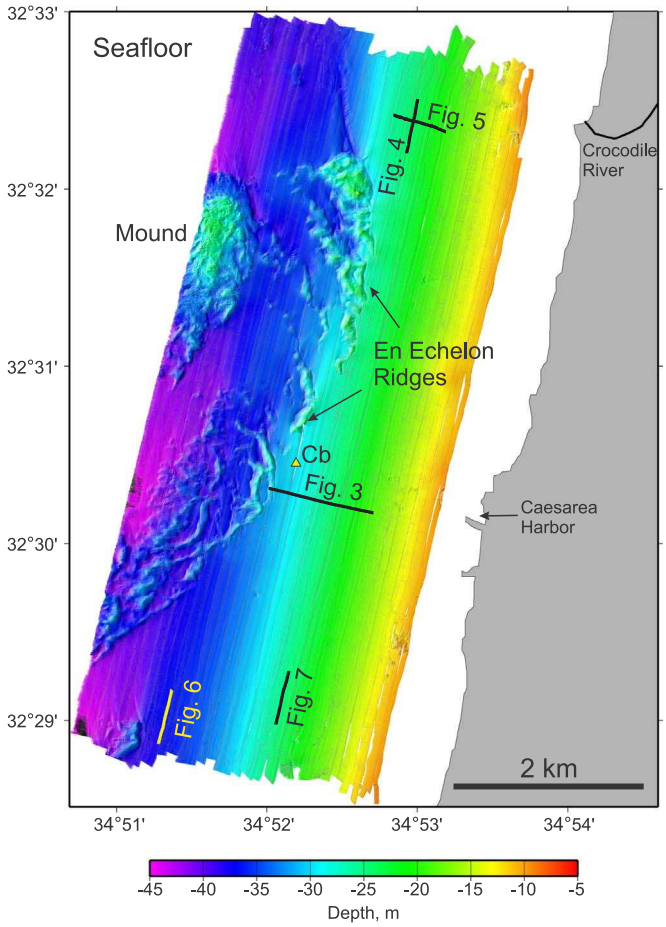

Fig. 2. Color-contoured multibeam bathymetry map of the survey area offshore Caesarea produced from the 2015 survey, artificially illuminated from the WNW. Location shown in Fig. 1. Locations for chirp seismic profile figures are indicated. "Cb" identifies offshore location of core with age dates discussed in Stienberg et al. (2016), see also Fig. 1.

of Caesarea's harbor (Reinhardt et al., 2006; Goodman-Tchernov et al., 2009; Dey and Goodman 2010; Dey et al., 2014; Goodman-Tchernov and Austin, 2015, Tyuleneva et al., 2017). Tsunami deposits identified to date that impacted Caesarea include six events occurring at 6, 3.5, 1.8, 1.4, 1.2, and 1 ka (Goodman et al., 2009; Dey et al., 2014, Tyuleneva et al., 2017). These distinctive, coarse-grained layers might also serve as a protective layer against further erosion down to any underlying prehistoric anthropogenic features.

The abundance of already interpreted and published data from archaeological, sedimentological and geophysical studies nearby provide a useful mosaic of defined sequences from which a more large-scale effort can benefit (Boyce et al., 2004; Boyce et al., 2008; Goodman et al., 2009; Raban, 2009; Shtienberg et al., 2014, 2016; Goodman-Tchernov and Austin, 2015; Roskin et al., 2015). The primary objective of the 2015 combined multibeam-chirp study was to incorporate existing knowledge with extensive, comprehensive multibeam and shallow subsurface feature mapping to reconstruct the broader early post-LGM offshore landscape, in order to predict potential habitats of prehistoric peoples who would have preferentially exploited the coastal rivers and associated estuaries for their natural resource richness and trade network access (Bailey and Flemming, 2008).

2. Methods

The multibeam bathymetry and chirp seismic reflection survey was conducted in September 2015, aboard the R/V *Mediterranean Explorer*, a 20.6 m research vessel operated by EcoOcean. The survey (Fig. 1), conducted with both instruments simultaneously, spanned ~8 km along the coast in water depths from ~10–45 mbsl. Strike lines numbered 37, at mostly ~100 m spacing, narrowing to ~50 m on the shallowest 8 profiles, to ensure the fullest bathymetric coverage. Dip profiles numbered 50, were ~3.3 km long, and spaced at ~200 m in the southern two-thirds of the survey and ~100 m in the northern third. Ship speed was maintained at ~4.5 kts.

Multibeam bathymetry data were collected using a Reson 7101 system, operating at 240 kHz with a 150° swath of coverage, and processed using CARIS software. Navigation was conducted using differential GPS, with attitude control by means of an Applanix POS MV inertial motion unit; the raw multibeam data were corrected for heave, pitch, roll and yaw. Sound velocity casts were collected periodically during the survey and utilized in processing to determine water depths from soundings. Tide corrections were performed based on time-series elevation data at the Hadera power plant (Fig. 1), obtained from the UNESCO/IOC sea level station monitoring facility (http://www.ioc-sealevelmonitoring.org/station.php?code=hade). Erroneous echo-sounder pings, recognizable by large positive or negative anomalies from the norm, were manually edited using both swath and subset editing modes within CARIS software. Navigation data were also edited within CARIS, and the multibeam lines were merged and motion data applied to correct for heave, pitch, roll and yaw. The final edited data were binned and gridded at 1 m, which is approximately the horizontal accuracy of the data. Only strike lines were used to eliminate artifacts created by small errors in vertical corrections on dip profiles. Vertical resolution errors in the final data average ± 10–20 cm. (Fig. 2).

Chirp seismic reflection data were collected using an Edgetech 216 towfish operating with a 20 ms, 2–12 kHz swept-frequency pulse at a 5 Hz ping rate. These data can image surficial subsurface layering at sub-decimeter resolution. Both full-waveform and envelope records were collected; however, the full-waveform data were found to display greater clarity for seismic stratigraphic analysis, whereas the envelope records generated better images at larger scales. Processing was conducted using Paradigm's Focus software, and included the following steps: heave filtering, corrections for fish depth (measured with an independent pressure gauge attached to the towfish) seafloor horizon mis-ties (which effectively provided a tide correction), trace equalization and water column muting. Navigation was also corrected for estimated layback of the towfish from the GPS antenna. Processed chirp data were imported into Landmark's DecisionSpace software for post-survey interpretation of seismic horizons. A sound speed of 1500 m/s was used for estimating horizon depth below sea level, while 1700 m/s was used for estimating thickness between horizons for preparation of isopach maps. Gridded structure maps and isopachs between horizons were generated by interpolation/extrapolation using a spline-in-tension algorithm (Wessel and Smith, 1998), masked outside of 80 m from grid nodes where each horizon was observed.

3. Results

3.1. Stratigraphic framework

Our investigation into the morphology and evolution of the shallowly submerged landscape offshore of Caesarea benefits from the fact that the main stratigraphic elements have been previously interpreted by Shtienberg et al. (2016), using similar chirp data combined with an analysis of coring results immediately south of our survey area (Fig. 1). We can correlate seismic horizons and facies observed in our study with those observed by Shtienberg et al. (2016), allowing us to begin our analysis from an *a priori* general understanding of the stratigraphic framework. Those elements are illustrated in Fig. 3.

The lowermost observable reflector is the top of the interpreted aeolianite basement, also referred to commonly as kurkar (Fig. 3); we label this reflector "K". This aeolianite is for the most part sandstone deposited during different periods ranging from ~183–58 ka

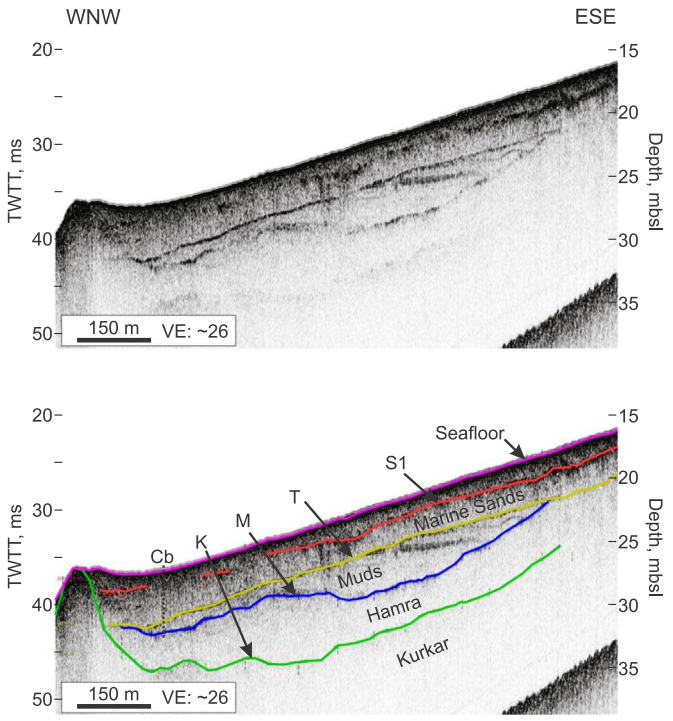

Fig. 3. Uninterpreted (top) and interpreted (bottom) acoustic reflection image of the envelope chirp record along a 2015 dip profile. Location shown in Fig. 2. Horizon interpretations "T", "M" and "K" are based on work of Shtienberg et al. (2016), with modified nomenclature (see text). Horizon "S1" is an intermittent, high amplitude reflector within the interpreted marine sequence above the "T" horizon. "Cb" identifies nearest location to that core, with age dates on clayey sediments between T and M discussed in Shtienberg et al. (2016).

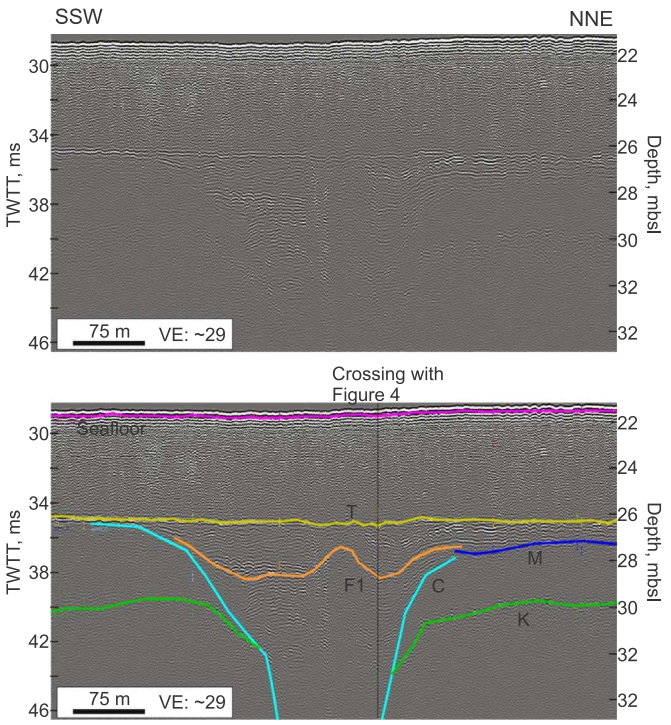

Fig. 4. Uninterpreted (top) and interpreted (bottom) chirp full-waveform acoustic reflection image crossing filled paleo-channel structure (whose base is the C horizon) in the northern sector of the survey, along a strike (along-shore) orientation. The "S1", "T", "M" and "K" horizons are as in Fig. 3. The "F1" horizon is defined as the topmost seismic reflector in the interpreted fill unit fully contained within the incision. Location shown in Fig. 2.

(Gvirtzman et al., 1998; Frechen et al., 2001; Porat et al., 2003, 2004; Sivan and Porat, 2004; Zviely et al., 2006; Mauz et al., 2013), and subsequently lithified by carbonate cementation to preserve the original ridge morphology (e.g., Porat et al., 2004; Mauz et al., 2013). On land and just offshore (Fig. 1), these ridges are oriented parallel to the shore (Tsoar, 2000; Sivan and Porat, 2004; Porat et al., 2004), and are hypothesized to have formed as coastal foredunes (Tsoar, 2000; Mauz et al., 2013) prior to lithification. The ridged morphology persists in the submarine environment (Zviely et al., 2006; Boyce et al., 2009; Schattner et al., 2010; Goodman-Tchernov and Austin, 2015; Figs. 2, 3), suggesting lithification prior to submergence. Overlying this acoustic basement is a silty sand layer identified by Shtienberg et al. (2016) as the Hamra unit; these terrestrial/paleosol sediments range in age from ~87 to ~55 ka on land (Porat et al., 2003; Sivan and Porat, 2004).

Overlying the Hamra unit in most (but not all) areas are dark, muddy (silty clay) sediments that are interpreted as wetlands units deposited prior to shoreline transgression (Shtienberg et al., 2016). The origin of these sediments is a topic of debate addressed in the discussion; here, we ascribe a generic identifier "M" to indicate the seismic reflector at the base of this unit (Fig. 3). In seismic section, this unit is often characterized by subhorizontal to slightly seaward-dipping reflectors that onlap the Hamra unit and are truncated by a strong erosional unconformity at the top (Shtienberg et al., 2016; Fig. 3), which we identify as the "T" reflector. Overlying these muddy sediments, and the Hamra unit where it is not present, are post-transgressive marine sands (Shtienberg et al., 2016); the erosional contact at the base of these sands elsewhere represents a transgressive ravinement caused by the shoreface migrating landward across the shelf (e.g., Duncan et al., 2000; Nordfjord et al., 2006; Goff et al., 2015). Shtienberg et al. (2016) recognized some reflectors within the marine sands above "T". We identify one high-amplitude reflector within these sands, labeled S1 in Fig. 3. This reflector may be associated with a tsunamite deposit (Goodman-Tchernov and Austin, 2015; Tyuleneva et al., 2017).

3.2. Paleo-channels

Our chirp seismic survey imaged two buried paleo-channels, one to the north, which we interpret as the ancestral course of the Crocodile River, and one to the south, which may represent the ancestral Hadera River (see Section 3.3). The northern paleo-channel is shown in Fig. 4; here, the paleo-channel is ~15 m deep (extending off the bottom of the section shown) and > 200 m wide across the top. Paleo-channels of this scale have not been observed or described previously anywhere along this coastline. We identify the reflector defining the base of the paleo-channel as "C"; this reflector is observed to be contiguous with the "M" reflector near the truncated top of the incision on the NNE side (Fig. 4). We observe the "K" reflector (i.e., top of the kurkar basement, see Fig., 3) to dip downward before it is truncated by "C" (Fig. 4). This observation suggests the longevity of the incision at this location, as it indicates fluvial (i.e., subaerial) erosion of the aeolianite foredune, followed by deposition of the Hamra ("M"-"K", Fig. 3) unit, and subsequent erosion of the Hamra unit and deepening of the incision into the aeolianite.

The paleo-channel fill above reflector "C" exhibits an undulating, complexly laminated seismic facies, suggesting multiple cut-and-fill episodes; the latest stages of these fill units are contiguous with the muddy interval ("T"-"M") that is present beyond the limits of the incision (Fig. 4). We identify a reflector "F1″ that we interpret as the transition from in-fill deposits below, that are confined to the paleo-channel, to deposits above that extend beyond the incision (Fig. 4). In this locale, during the latest stages of infilling, the paleo-channel morphology transitioned from a single incision to a double channel, each appearing to aggrade upward (Fig. 4). The nature of "F1" is further illustrated on a dip profile that crosses Fig. 4, as well as numerous additional strike profiles (Fig. 5). Fig. 5 demonstrates that "F1", as

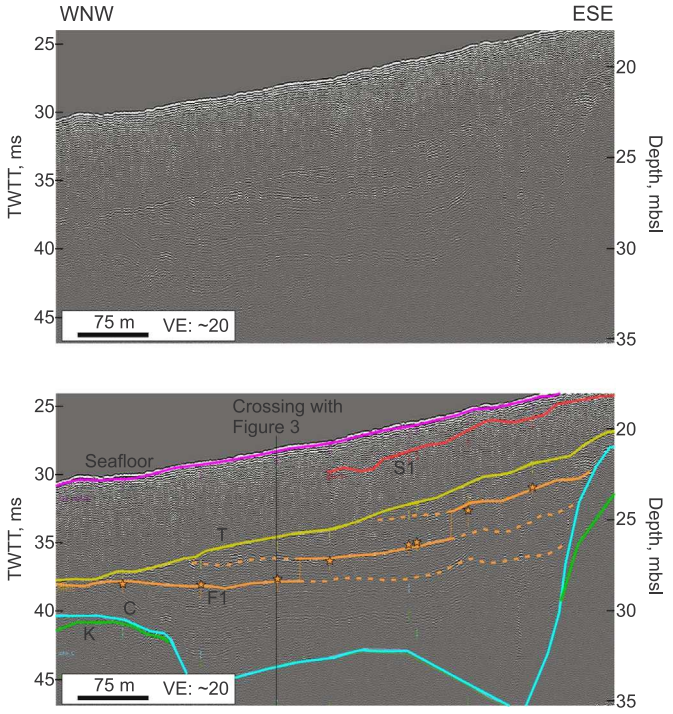

Fig. 5. Uninterpreted (top) and interpreted (bottom) acoustic reflection image of the full-waveform chirp record crossing filled paleo-channel structure ("C" horizon) in the northern sector of the survey along a dip (cross-shore) orientation, thus cutting obliquely across the ~shore-perpendicular channel. The "S1", "T", and "K" horizons are as in Fig. 3. The pick for the "F1" horizon appears to step up at several inferred locations in order to correlate with the crossing strike-line interpretations for this horizon; cross-line interpretations for "F1″ are shown by orange stars (corrected for seafloor offsets between crossing lines). "F1" must therefore be multiple off-lapping surfaces, the updip and downdip continuations of which are indicated by dashed lines. Location shown in Fig. 2.

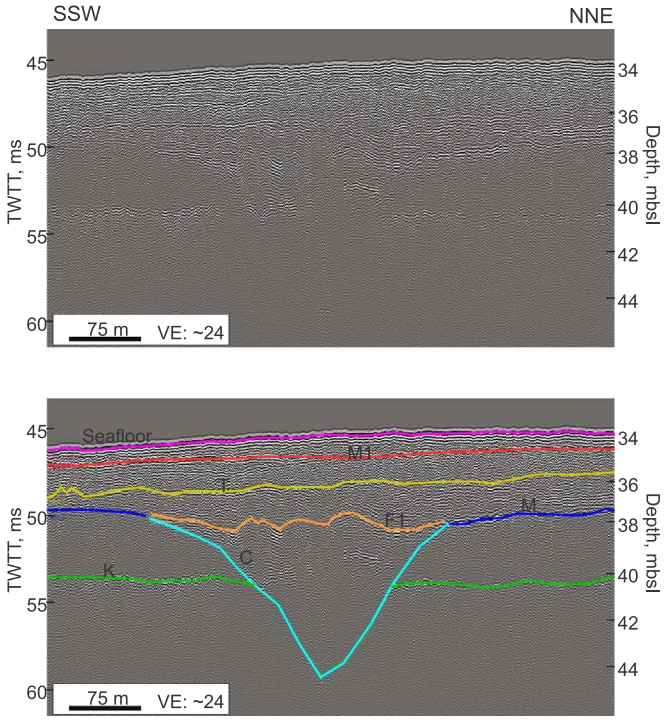

Fig. 6. Uninterpreted (top) and interpreted (bottom) full-waveform chirp record crossing another filled paleo-channel (defined at its base by a reflector we term "C") in the southern sector of the survey along a strike (along-shore) orientation, at ~34 m water depth. The "S1", "T", "M" and "K" horizons are as in Fig. 3. The "F1" horizon is again defined as the topmost seismic reflector in the interpreted fill unit, fully contained within the channel. Seismic facies of fill units below "F1" observed here are generally similar to fill units of the northern paleo-channel. Location shown in Fig. 2.

defined above for each strike-line crossing of the paleo-channel, is not a single horizon in the offshore direction. Rather, it consists of multiple subhorizontal to slightly seaward-dipping, shingled horizons that step up toward the shore; each onlaps landward onto the flanks of the paleo-channel, and is truncated to seaward by the transgressive ravinement ("T").

The seismic facies of the fill deposits within the northern paleo-channel exhibit a similar character on all crossings (i.e., undulating, complexly laminated). However, we observe spatial differences within the southern paleo-channel. A deep (~34 m water depth) crossing of this feature is shown in Fig. 6. The southern incision is not as deep as the northern one; on Fig. 6, it is only ~6 m. The widths are comparable, > 200 m at the top, and the fill facies similarly consist of undulating laminated reflectors, merging above and beyond the F1 reflector with the broader interpreted estuarine ("T"-"M") deposits. Along a shallower (~23 m water depth) chirp crossing (Fig. 7), we observe similar horizontal and vertical scales of the incision, but the fill facies below the F1 reflector are lower amplitude chaotic, rather than laminated. At shallower water depths, this paleo-channel becomes seismically poorly defined.

3.3. Horizon synthesis

3.3.1. Structure maps

The seafloor bathymetry (Fig. 2) represents the uppermost surface mapped within the seismic stratigraphic framework in our survey area. Numerous aeolianite/kurkar outcrops are evident, most prominently a set of arcuate, *en-echelon* ridges at depths ~40–25 mbsl, as well as a massive (~20 m high, ~4 km long, ~1 km wide) teardrop-shaped mound whose base is at ~40 mbsl. A more complete picture of the aeolianite morphology is provided by the structure map for the "K"

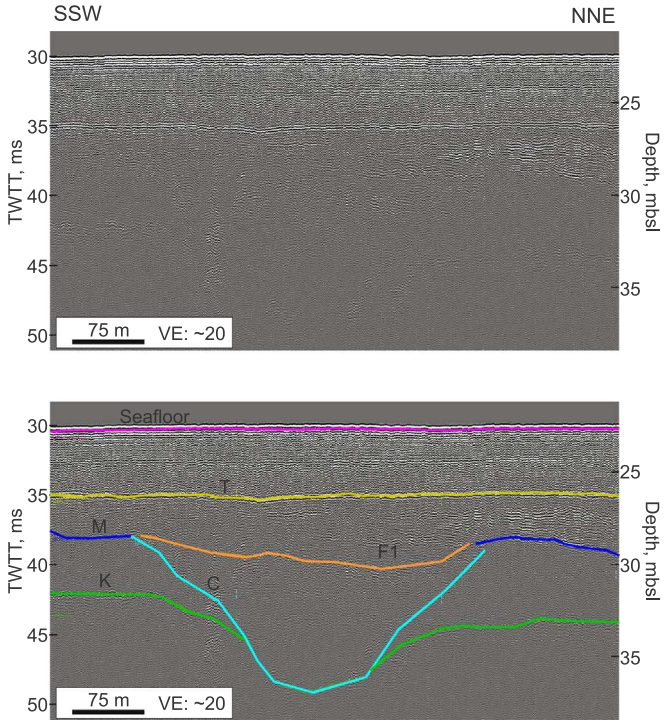

Fig. 7. Uninterpreted (top) and interpreted (bottom) full-waveform CHIRP record crossing filled channel structure (defined by "C") in the southern part of the survey along a strike (along-shore) orientation, at ~23 m water depth. The "T", "M" and "K" horizons are as in Fig. 3. The F1 horizon, here broadly "U"-shaped, is again defined as the topmost seismic reflector in the fill unit fully contained within the channel. Seismic facies of fill units in this crossing are chaotic and only weakly reflective. Location shown in Fig. 2.

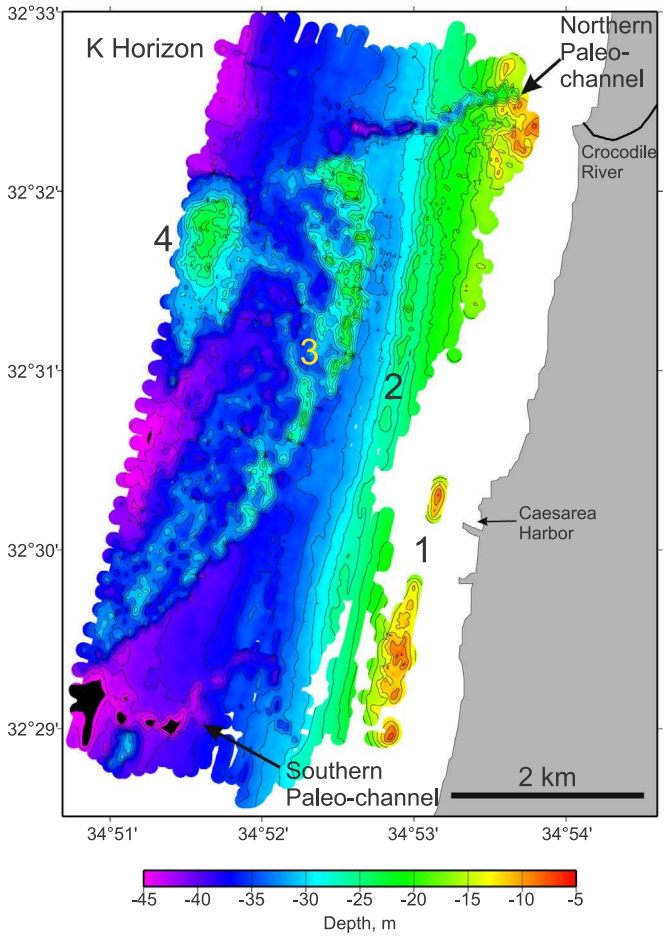

Fig. 8. Structure map of the "K" (top kurkar/aeolianite basement) horizon, both color-contoured and line-contoured (2-m intervals). Numbers identify four distinct aeolianite ridge complexes. Note how the northern paleo-channel erodes the kurkar ridges/basement, as is also indicated on Fig. 4.

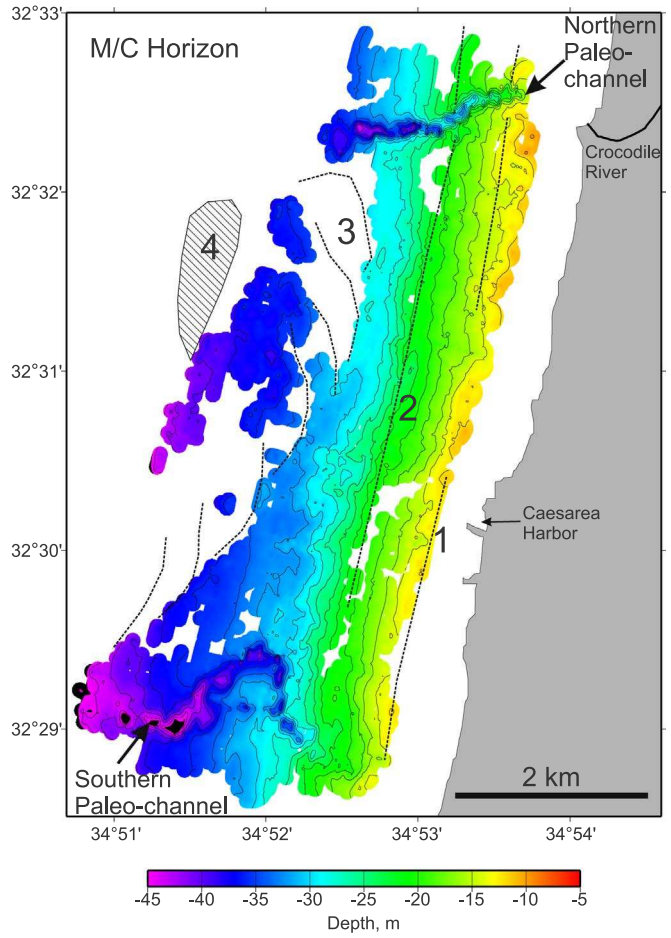

Fig. 9. Structure map of the combined "M" (mud base) and "C" (channel base) horizons. Outlines of the interpreted four aeolianite ridge complexes (Fig. 8) are overlain.

horizon (Fig. 8), which effectively strips off the sediment overburden (although the "K" horizon is not always well imaged in shallower water depths). We identify in this map four distinct aeolianite ridge complexes, which are numbered in Fig. 8. The shallowest ridge complexes, 1 and 2, are shore-parallel, similar in morphology to aeolianite ridges observed nearshore (Fig. 1) and on land (Tsoar, 2000; Sivan and Porat, 2004; Porat et al., 2004). Ridge complexes 3 (arcuate, *en-echelon* ridges) and 4 (massive, teardrop-shaped mound) are different, representing significant departures from what is considered kurkar ridge morphology along the modern Israeli coast.

The northern and southern paleo-channels are also expressed in the "K" horizon structure map (Fig. 8), but are more completely imaged by "C", which is combined with "M" to form a combined structure map in Fig. 9. The northern paleo-channel is well imaged, almost to the chirp profiles in shallowest water (~10 m), and can clearly be linked to the modern Crocodile River where it intersects the coastline just north of an aeolianite headland (Figs. 1 and 9). Therefore, we conclude that the northern paleo-channel represents the ancestral course of the Crocodile River at lowered sea-level during glacial (LGM) and early post-glacial conditions. This paleo-channel is slightly oblique with respect to modern bathymetric contours, displaying little sinuosity. The subsurface expression of the northern paleo-channel is not evident below ~35–40 mbsl (Fig. 9). In contrast, the southern paleo-channel exhibits substantial sinuosity, and is most clearly observed in deeper water depths (~20–40 mbsl; Fig. 9). At shallower depths, this paleo-channel is smaller and weaker in seismic expression. Nevertheless, the trend of this buried incision as it approaches the coastline (Fig. 9) is directed toward the present-day Hadera River channel, where it existed prior to diversion by construction of the power plant (Fig. 1). Shtienberg et al. (2016), in their survey just to the south, generated structure maps which they also purported to show evidence of channeling, arguing that these features represented ancestral drainage from the Hadera River. However, the features that they identified are smaller than the southern paleo-channel observed in our survey; we conclude that our southern paleo-channel is a more likely candidate for accommodating the primary Hadera River flow at relative lowstand conditions.

In the region between the two paleo-channels, particularly between aeolianite ridges complexes 2 and 3 (Fig. 9) where several basins provide accommodation space, the "M"/"C" structure map suggests that ponding of muddy sediments has occurred. Although ridge complex 2 is fully covered by Hamra deposits, it nevertheless appears to exert a strong influence on morphology of the "M" horizon, as evidenced by steepening of the slope along the seaward flank of this shore-parallel ridge (Fig. 9). Ponding of muddy sediments is also observed between ridge complexes 1 and 2, though to a lesser extent.

The "T" horizon (Fig. 10) does not exhibit significant along-strike structure; instead, it deepens monotonically seaward. This interpreted transgressive ravinement effectively erases preexisting subsurface structures, except where the aeolianite basement stands above the modern seafloor.

3.3.2. Isopach maps

The isopach map indicating the thickness of interpreted muddy sediments ("T"-"M"/"C") is displayed in Fig. 11. These sediments are thickest within the two paleo-channels, but are present throughout the survey area landward of aeolianite ridge complex 3, and also within

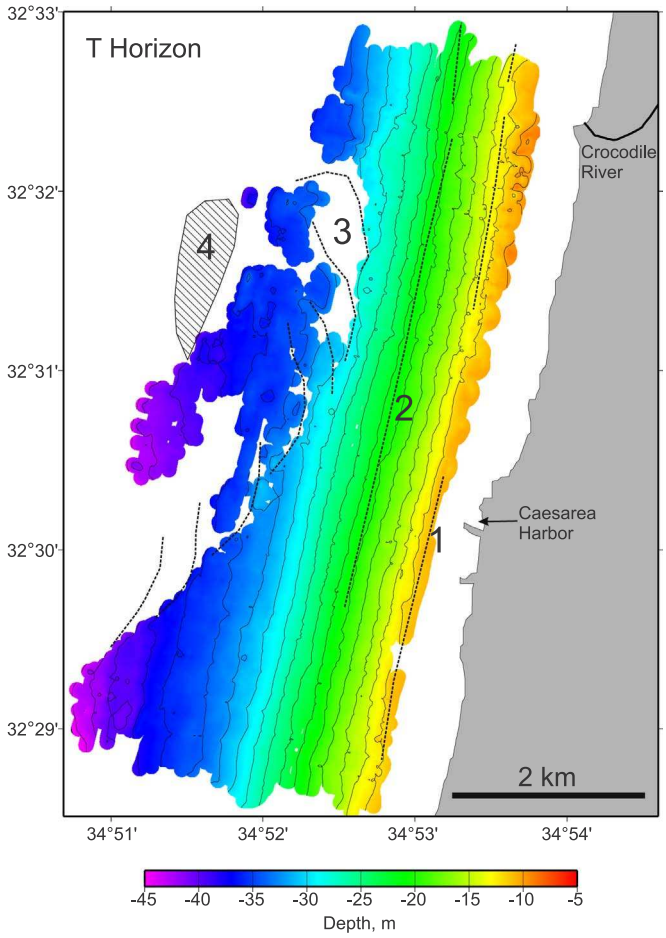

Fig. 10. Structure map of the "T" (interpreted transgressive ravinement) horizon. Outlines of the four aeolianite ridge complexes (Fig. 8) are overlain.

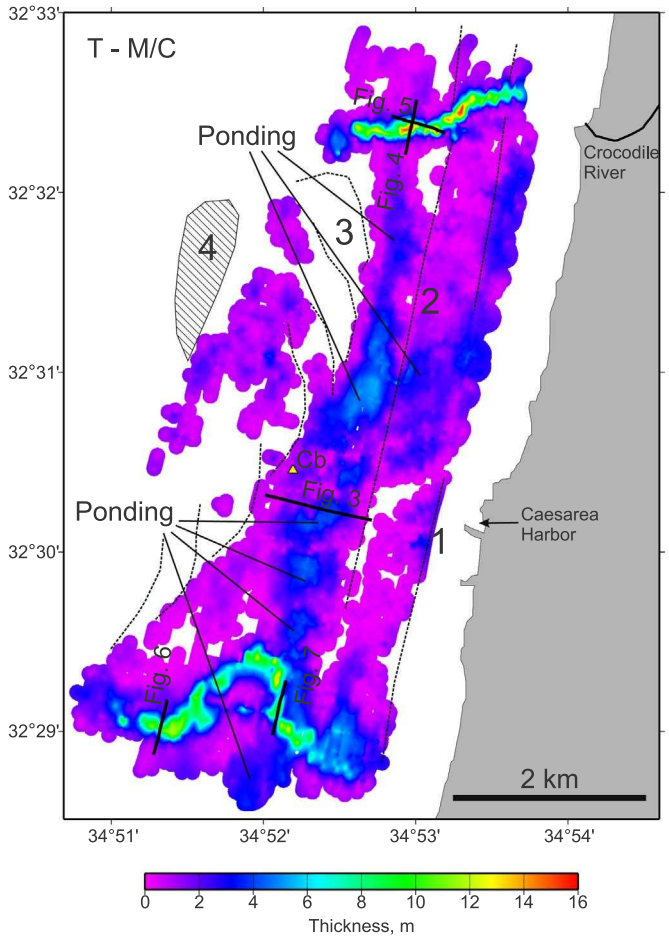

Fig. 11. Color-contoured isopach map of the estuarine sediments between the "M"/"C" and "T" horizons. Outlines of the four aeolianite ridge complexes (Fig. 8) are overlain. "Cb" identifies the location of a core with age dates on this clayey unit discussed in Stienberg et al. (2016).

some isolated areas between ridge complexes 3 and 4 (Fig. 11). The thickest accumulations outside of where the paleo-channels occur define a trend of sediment ponds (Fig. 11); in the northern half of the survey, these are located just landward of ridge complex 3, but they diverge to the south where that ridge complex trends toward deeper water. Additional ponds are located in shallower water.

The thickness of the interpreted marine sand sheet (Seafloor-"T") is displayed in Fig. 12. This unit is thickest along a band in the northern part of the survey that tracks closely with the muddy sediment ponding noted in Fig. 11, thinning both to seaward and landward.

4. Discussion

4.1. Terrestrial versus estuarine origin for muddy sediments

Analysis of a core into the Maagen Michael fishponds on land (Fig. 1) just north of our study area along the Israeli coast (Cohen-Seffer et al., 2005; Sivan et al., 2011) has revealed terrestrial wetland deposits from a freshwater marsh overlying Hamra paleosols. These sediments were deposited within an aeolianite basin over a brief (~1000 yr) period of time ending 9.43 ka (Sivan et al., 2011). Other freshwater wetland deposits of similar age have been cored along the central and northern Israeli coastal plain (Kadosh et al., 2004; Zviely et al., 2006). At the time these clayey sediments were deposited, sea level was ~50 m lower than it is today (Lambeck et al., 2014; Shackleton, 1987); the wetland environments associated with these deposits could not have been connected to the marine environment, and therefore they are not a part of the Holocene transgressive systems track.

Shtienberg et al., (2016, 2017);) argue that offshore mud deposits they have sampled stratigraphically correspond to these terrestrial wetlands deposits. They have, however, only one datum to support this correspondence: a similar date (10.7–9.4 ka) from a mud unit that was sampled in core "Cb" (Neev et al., 1976), located directly offshore of Caesarea (Fig. 2) in water depths that indicate the date is from a sample from the deepest portion of our interpreted "T"-"M"/"C" muddy unit (Figs. 3, 11). The interpretation by Shtienberg et al., (2016, 2017) suggests that muddy/wetlands sediments onshore and offshore were deposited concurrently, with no variation as a function of ambient water depth, nor linkage to a rising sea level and transgressing coastline. However, the observed seismic stratigraphy contradicts this prediction. In particular, landward-onlapping/gently shingled layers (Figs. 3, 5) within fill of our northern paleo-channel are characteristic of a transgressive estuarine sequence (Allen and Posamentier, 1993), where older layers were deposited at greater depth/distance from shore and younger layers at shallower depth/shorter distance from shore, modulated by the accommodation space provided by rising sea level and the advancing shoreline (Fig. 13). Although the interpreted muddy unit tends to localize in isolated ponds (Fig. 11), within the fill unit of the northern paleo-channel, we can document continuous deposition from ~35 mbsl to ~10 mbsl, progressing older-to-younger in stratigraphic age with decreasing water depth (Fig. 5). Therefore, we interpret the offshore muddy deposits sampled by Shtienberg et al. (2016) to be estuarine in origin. This interpretation is consistent with the 10.7–9.4 ka age range for these sediments reported both by Neev et al. (1978) and Shtienberg et al. (2016), because the depth at which these mud samples were taken (~32 mbsl) corresponds to an age of ~9.6 ka

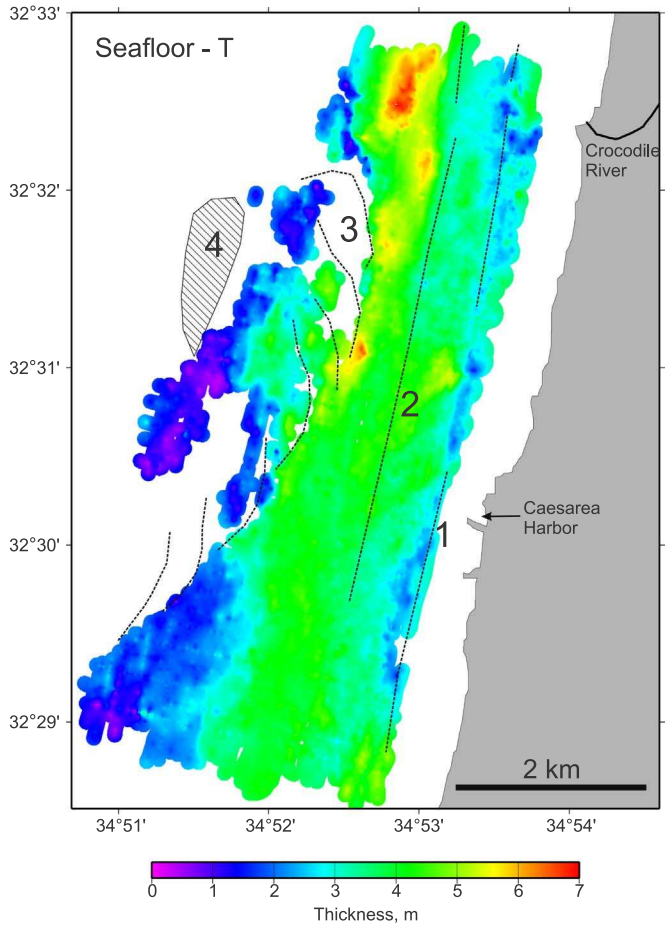

Fig. 12. Color-contoured isopach map of the marine sand sediments between the "T" horizon and the seafloor. Outlines of the four aeolianite ridge complexes (Fig. 8) are overlain.

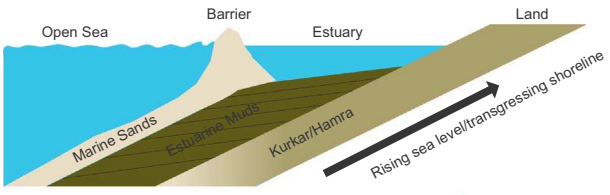

Fig. 13. Schematic illustration for the formation of stacked, landward-onlapping horizons within estuarine muds created by rising sea levels and transgressing shoreline and barrier island.

on the local sea level curve (Schattner et al., 2010), suggesting proximity of the ambient shoreline to these sediments when they were deposited.

Further evidence for an estuarine origin for the interval in question comes from the fact that seismically laminated, interpreted muddy fill units within the paleo-channels, likely fluvial (subaerial) sediments as a result of our correlation of these paleo-channels to onshore river systems, must have preceded deposition of the interpreted estuarine sediments across the broader shelf. Fine-grained deposition within, and eventual filling of, a river channel requires a transition from fluvial to estuarine conditions that accompanies an approaching coastline (Dalrymple et al., 1992; Allen and Posamentier, 1993; Buck et al., 1999). Furthermore, the undulating, aggradational character of the channel-fill strata (Figs. 4, 6) is suggestive of deposition under tidal influence (Allen and Posamentier, 1993; Tessier et al., 2012). Thus, we conclude that the broader depositional environment which post-dates the channel-fill existed proximal to a shoreline.

4.2. Estuary formation

We hypothesize that estuary formation was facilitated in this offshore part of the Israel coast by the presence of barrier islands, providing protection of the estuary(ies) against storm reworking (Figs. 13, 14). Once the observed paleo-channel/ancestral river valleys were filled, fine-grained deposition (likely from the Crocodile and Hadera river systems) would have extended along the shelf outside of these channels (Figs. 5, 6, 7, 11, and 14) by mechanisms of longshore drift, as is known today. There would have been neither protection from storms nor accommodation space available without seaward barriers. Submerging aeolianite ridges would have provided such barriers at first (Figs. 8, 9, 14). Ridge complex 3, for example, rises up to ~10 m above the surrounding seafloor; these features would have been offshore islands when sea level was ~30–20 m below the modern level (~9.5–9.0 ka; Schattner et al., 2010; Lambeck et al., 2014). Indeed, some of the deepest ponding of interpreted muddy sediments occurs between ridge complex 3 (seaward) and ridge complex 2 (landward; Fig. 11). However, south of latitude 32°30′N, ridge complex 3 bends westward toward greater water depths, whereas the observed trend of mud-filled basins continues southward along the coast, crossing the southern paleo-channel (Fig. 11). Ridge complex 2 could be considered a landward buttress for these basins, allowing for deepening of these southern sediment accumulations, but there is no aeolianite ridge seaward in the southern part of the study area to prevent sediment escape to deeper water and destruction of estuarine deposits by the transgressing shoreline. Outside of the deepest sediment ponds, the muddy (interpreted estuarine) unit is broadly present at varying thickness across all water depths (Fig. 11). We also do not observe evidence of basins in the structure map of the "M"/"C" horizon between ridge complexes 1 and 2 (Fig. 9); the region between those two ridge complexes is filled with older Hamra deposits; apparently, those sediments did not provide accommodation space for later (i.e., Holocene) estuary formation.

From these indirect observations, we infer that barrier islands constructed from mobile sands, either eroding from the lithified kurkar basement, being supplied by the ambient rivers systems, and/or replenished by the Nile system, played an important role in estuary formation along the coast during Holocene sea level rise (Fig. 14). We speculate that the shallowest portions of aeolianite ridge complex 3, which was likely being eroded by rising sea level, provided an anchor for development of a larger barrier island that extended north and south along-shore at that water depth, providing accommodation space for the largest observed sediment ponds outside the paleo-channels (Figs. 9, 11, and 14). As sea level rose and this aeolianite ridge system was overtopped, the sand barrier would have migrated shoreward (e.g., Thorne and Swift, 1991), shifting the locus of estuarine sedimentation landward (Fig. 14). The marine sand isopach map (Fig. 12) supports this scenario, because these sands are not uniformly distributed across the shelf, but rather are observed to be thickest (~4–7 m) along a band that closely overlies the band of deepest muddy sediment ponding (Fig. 11). Where a beach barrier is present at the coast, the transgressive marine sand sheet is formed by the transfer, through shoreface erosion, of barrier sands to the inner shelf, overlying the transgressive ravinement created by this erosion (Thorne and Swift, 1991). Therefore, the thicker zone of sand we observe is likely the transgressive residue of the barrier island(s) that fronted the estuary at the time.

The seismic facies of the fill units ("F1"-"C") in the southern paleo-channel undergo a change from undulating/laminated at greater depth (Fig. 6) to weakly chaotic at shallower depth (Fig. 7). That change is approximately coincident with the seaward edge of the band of sediment ponding in the interpreted estuarine deposits (compare locations of Figs. 6 and 7 on Fig. 11). Without samples to confirm or refute, we can only speculate as to the nature of this transition. However, we suggest that the weakly chaotic facies could be coarser-grained, possibly fluvial sediments (Nordfjord et al., 2006). If so, it could indicate that delivery of sand to the coast through the southern (Hadera) river

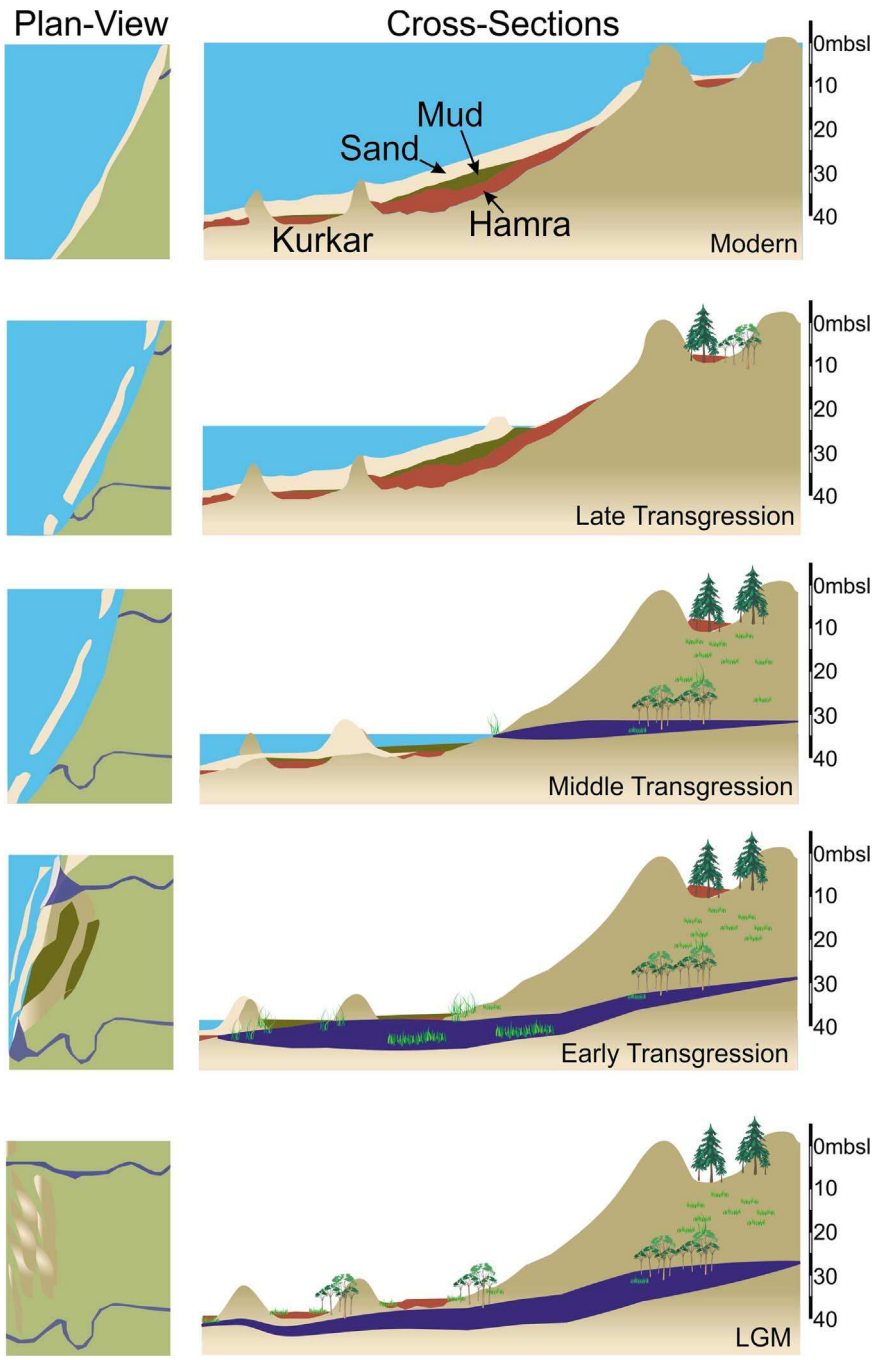

Fig. 14. Illustration of hypothesis presented here for formation of continental shelf stratigraphy offshore Caesarea, Israel, since LGM. See text for discussion.

was enhanced during the most significant period of estuarine development on the shelf.

4.3. Possible sources for barrier sands

The depth ranges over which we observe probable estuarine sedimentation, ~45 to ~10 mbsl, correspond to positions of sea level ~10.5–7.5 ka (Schattner et al., 2010; Lambeck et al., 2014), a period that includes some of the fastest rates of sea level rise experienced during the Holocene. This age range also includes the widely recognized meltwater pulse phase at ~8.2 ka (associated sea-level rise rate of ~1–1.7 cm/yr; Törnqvist et al., 2004; Schattner et al., 2010; Cronin, 2012; Lambeck et al., 2014 Goodman-Tchernov and Katz, 2016). A high rate of sea level rise is a destabilizing factor for the preservation of barrier islands, which require a large influx of sand as a counterbalance in order to maintain themselves and the estuaries they protect (FitzGerald et al., 2008). Coastal sands along the central Israeli coast today are sourced primarily from the Nile River, transported both by sea along the Nile littoral cell (Zviely et al., 2006; Schattner et al., 2010; Shtienberg et al., 2017) and blown landward by prevailing southwest to northwest winds (Tsoar, 2000). Shtienberg et al. (2017) have suggested that rapid sea level rise during the early Holocene could have led to increased erosion of the Nile Delta, and thereby provided a significant increase in sand fluxed to the coast by the Nile littoral cell during that time as well.

Shifts in climate are another potential factor in defining the evolution of estuarine conditions during the Holocene transgression. The early Holocene climate of the southeastern Mediterranean, from 10 to ~7 ka, was marked by much wetter conditions than today (Bar-Matthews et al., 2003; Langgut et al., 2011). These conditions could

have been concurrent with overall increased erosion of kurkar outcrops and sediment flux to the coast at the time, both coarse and fine-grained from the Nile as well as from local rivers (Woodward et al., 2008; Marriner et al., 2013). As suggested above, the weakly chaotic facies in the upper portions of the southern paleo-channel may be a marker of enhanced transport of fluvial sediments to the shelf, which would be consistent with this hypothesis.

4.4. Aeolianite/dune morphology

The *en echelon*, arcuate morphology of the ridges in aeolianite ridge complex 3 (Fig. 8) is both surprising and enigmatic. The shallower ridge complexes 1 and 2, as well as aeolianite ridges seen nearshore (Fig. 1) and on land (Tsoar, 2000; Sivan and Porat, 2004; Porat et al., 2004; Mauz et al., 2013), are all linear and parallel to the coast, and can be linked to coastal foredune processes (Tsoar, 2000; Mauz et al., 2013). The observed arcuate ridge complex thus indicates some sort of important change in dune-forming processes. Mauz et al. (2013) identify four discrete age groups for aeolianite ridges on land: ~183 ka, ~97 ka, ~74 ka, and ~58 ka, with the youngest ridges more seaward, such that an offlapping, downstepping stacking pattern can be inferred. Mauz et al. (2013) demonstrate that these foredunes are generated within ~10 km of the coast; when this distance is exceeded during progradation, sediment bypass occurs and a new foredune is formed several kilometers further out on the shelf. Thus, these aeolianite ridges can be linked to falling sea level, and the youngest three on-land ridge units can be associated with the prograding shoreline since the marine isotope stage (MIS) 5 highstands (Waelbroeck et al., 2002). Assuming that this age progression continues with depth, then the submerged ridge complexes 1–4 would have formed progressively younger, possibly approaching LGM ages (MIS 2) for complexes 3 and 4. Eastern Mediterranean climate was extremely cold and arid at this time (Langgut et al., 2011), and may be a contributing factor in altering the coastal dune-forming dynamics.

Given the prevailing westerly wind directions (Tsoar, 2000), the arcuate forms of ridge complex 3 resemble parabolic dunes (Pye and Tsoar, 2009). Parabolic dunes are identified as “blow-out” features (Pye and Tsoar, 2009; Abhar et al., 2015), whereby a resistant surface (typically vegetated) is breached in a location (blowout), allowing wind erosion to extract unconsolidated sand beneath and transport it downwind to form a dune. In the process, the resistant surface is progressively undercut on the downwind edge of the blowout, and both blowout and dune migrate downwind. The resulting dune shape is arcuate, surrounding the blowout, concave to the prevailing wind direction. A well-studied modern example of parabolic dunes is found within the Cape Cod National Seashore, MA, USA (Forman et al., 2008; Abhar et al., 2015). Prior to settlement by Europeans, Cape Cod was covered by a mature forest that inhibited dune formation (Forman et al., 2008). Clear-cutting and agricultural practices of the 17th and 18th centuries denuded most of the vegetation, allowing for mobility of the underlying sands and formation of dunes (Forman et al., 2008). The anthropogenically-initiated parabolic dunes of Cape Cod could be a clue to understanding why parabolic dunes initiated during MIS 2 on the Israeli coast. At this age, tree pollen counts in the eastern Mediterranean are at their lowest point compared to the previous 86 kyr, indicating very dry and cold conditions (Langgut et al., 2011). We speculate, therefore, that this climatic shift resulted in denudation of vegetation along the Israeli coast, allowing parabolic dune formation inland of the beach foredune. Subsequent cementation hardened these dunes to preserve their morphology during post-LGM transgression and submersion (see Section 4.2).

Ridge complex 4, a massive, teardrop-shaped mound at the seaward edge of our survey (Fig. 8), is a perplexing feature. Its form does not correspond to modern analog dune forms that we are aware of. The asymmetric shape suggests that it formed in the presence of south-directed, along-shore transport. However, that orientation is consistent neither with the expected westerly winds (Tsoar, 2000) nor the northward-directed Nile River littoral cell (Goldsmith and Golick, 1980; Zviely et al., 2007). Without additional information, we are unable to suggest an explanation for this feature.

4.5. Implications for ancient peoples

Worldwide, over 75 million km^2 of habitable land for humans was probably submerged by sea-level rise following the LGM (Gautney and Holliday, 2015; Benjamin et al., 2017). The post-LGM time period coincides with evidence for some of the most pivotal and critical cultural developments experienced by humans, including the advent of agriculture and the rise of complex societies (Sauer, 1952; Binford, 1968; Flannery, 1973; Hole, 1984; Bar-Yosef, 1998; Weisdorf, 2005; Putterman, 2008). Given the inclination for humans to occupy coastlines (Hinrichsen, 1996; Vitousek et al., 1997; Cohen and Small, 1997; Small and Nicholls, 2003), we can presume that a large proportion of human cultural heritage remains undiscovered and undocumented beneath now-submerged continental shelves. This dearth of knowledge is in part due to the technical, financial and logistical limitations of performing wide-scale underwater archaeological survey and excavation. Located sites on land can be similarly hidden from view, but in many cases are more easily discovered using aerial LIDAR, walking field surveys and even satellite technologies (Jones and Sarris, 2000; White and King, 2007; Parcak, 2009; Banning et al., 2017). The mere scale of investigation of an underwater site, by logistical necessity, tends to be much smaller, and the remains of prehistoric sites more ephemeral; therefore, any and all information that can concentrate examination efforts into the smallest area is critical for their discovery. The results here provide the framework and foundation for pinpointing places of higher potential in which coring or excavation efforts can be applied. There is significant precedence for this, given the discovery of concentrations of prehistoric lithic fragments in analogous deposits from Middle Paleolithic Mousterian (70–35 ka) and Epipaleolithic (17–11 ka) Hamra deposits along the Carmel coast of Israel to the north of Caesarea (Ronen, 1977; Tsatskin and Ronen, 1999). These inclusions are common enough to be regularly used for reconstructing the chronology of the Hamra and eolianite sequences along the Carmel coast of Israel (Farrand and Ronen, 1974). Human activities would have been very likely within and around our newly identified paleo-channels (i.e., ancestral river valleys) and within the flanking estuarine system, which would have been optimal for agriculture. Therefore, further targeted archaeological investigations, such as coring, excavations, or even higher resolution subbottom profiling concentrated in these areas, could produce evidence of prehistoric human presence.

5. Conclusions

Our morphologic and shallow stratigraphic investigation offshore of Caesarea, along the central Israeli shore, reveals significant changes in coastal sedimentary processes that we interpret as being associated with important climate changes over the latest Pleistocene-early Holocene in the southeast Mediterranean. Estuaries are nearly non-existent along the modern Israeli coast. However, our mapping of probable estuarine sediments offshore, both within paleo-channels/ancestral river valleys and more broadly deposited across the shelf, indicates that estuaries were likely widespread here during the early Holocene (~10.5–7.5 ka), when sea level was rising rapidly. Although offshore/now submerged aeolianite ridges provided some barrier protection against the open ocean for estuarine development, the ridges are insufficient to account for all of the estuaries that formed. We hypothesize that barrier islands developed to provide additional protection. This hypothesis is supported by the presence of a thickened marine sand sheet over areas where estuarine development was most prominent. We suggest two possibilities for higher sand delivery: (1) enhanced erosion of the Nile Delta during sea-level rise, transported

northward along the Nile littoral cell (Shtienberg et al., 2016), and/or (2) wetter conditions in the eastern Mediterranean during the early Holocene (Bar-Matthews et al., 2003; Langgut et al., 2011), allowing for greater erosion and transport of sediment to the coastline by local rivers.

The abundant aeolianite ridges along the Israeli coastline, both on shore and submerged, represent wind-derived dunes subsequently cemented to preserve their morphology (Gvirtzman et al., 1998; Frechen et al., 2001; Porat et al., 2003, 2004; Sivan and Porat, 2004; Zviely et al., 2006; Mauz et al., 2013). On land and in shallow water depths, these features are linear, parallel to the coast; we hypothesize that they formed as coastal foredunes during pre-LGM regression (Tsoar, 2000; Mauz et al., 2013). However, below ~30 m water depth in our survey area, a series of arcuate, nested ridges exhibit instead the morphology of parabolic dunes (Pye and Tsoar, 2009). Given the younging-to-seaward progression of ridge ages on land reported by Mauz et al. (2013), these parabolic dunes likely formed near the beginning of MIS2, which is associated with a transition to very dry and cold conditions in the eastern Mediterranean (Langgut et al., 2011). By analogy with recently-initiated parabolic dunes of the Cape Cod National Seashore, in MA, USA (Forman et al., 2008), we speculate that arboreal denudation associated with the known climatic shift enabled parabolic dune formation inland from the preexisting coastal foredune complex.

The presence of preserved estuarine sediments, along with filled ancestral river valleys, promise a trove of rich archaeological discoveries along this submerged coast as such excavations continue.

Acknowledgements

The survey was primarily supported by a seed grant from the Jackson School of Geosciences, The University of Texas/Austin (Goff and Austin) and Norman Krischer of Montclaire, NJ (Goodman-Tchernov). We thank M. Davis and S. Saustrup of UTIG for their technical support in collecting and processing the geophysical data. Field assistance from N. Hoffmann, O. Katz, T. Katz, R. Jaijel, N. Tyuleneva, and support from the University of Haifa Marine Geoarchaeology and Micropaleontology lab members was also appreciated. We also thank EcoOcean, and especially the captain and crewman of the R/V *Mediterranean Explorer*, for their assistance and seamanship in making the survey a success. UTIG Contribution #3265.

References

Abhar, K.C., Walker, I.J., Hesp, P.A., Gares, P.A., 2015. Spatial-temporal evolution of aeolian blowout dunes at Cape Cod. Geomorph 236, 148–162.
Allen, G.P., Posamentier, H.W., 1993. Sequence stratigraphy and facies model of an incised valley fill: the Gironde Estuary, France. J. Sed. Pet. 63, 378–391.
Banning, E.B., Hawkins, A.L., Stewart, S.T., Hitchings, P., Edwards, S., 2017. Quality assurance in archaeological survey. J. Archaeol. Method Theory 1–23.
Bar-Matthews, M., Ayalon, A., Gilmour, M., Matthews, A., Hawkesworth, C.J., 2003. Sea-land isotopic relationships from planktonic foraminifera and speleothems in the Eastern Mediterranean region and their implication for paleorainfall during interglacial intervals. Geochim. Cosmochim. Acta 67, 3181–3199.
Bar-Yosef, O., 1998. On the nature of transition: the Middle to Upper Palaeolithic and Neolithic revolution. Camb. Archaeol. J. 8, 141–177.
Benjamin, J., Rovere, A., Fontana, A., Furlani, S., Vacchi, M., Inglis, R.H., Galili, E., Antonioli, F., Sivan, D., Miko, S., Mourtzas, N., Felja, I., Meredith-Williams, M., Goodman-Tchernov, B., Kolaiti, E., Anzidei, M., Gehrels, R., 2017. Late Quaternary sea-level changes and early human societies in the central and eastern Mediterranean Basin: an interdisciplinary review. Quat. Int. http://dx.doi.org/10.1016/j.quaint.2017.06.025.
Binford, L.R., 1968. Early Upper Pleistocene adaptations in the Levant. Am. Anthropol. 70, 707–717.
Boyce, J.I., Reinhardt, E.G., Pozza, M.R., 2004. Marine magnetic survey of a submerged Roman harbour. Int. J. Naut. Archaeol. 33, 122–136.
Boyce, J.I., Reinhardt, E.G., Pozza, M.R., Goodman, B.N., 2009. Magnetic detection of ship ballast deposits and anchorage sites in King Herod's Roman harbor, Caesarea Maritima. Isr. J. Archaeol. Sci. 36, 1516–1526.
Buck, K.F., Olson, H.C., Austin Jr., J.A., 1999. Paleoenvironmental evidence for latest Pleistocene sea-level fluctuations on the New Jersey outer continental shelf: combining high-resolution sequence stratigraphy and foraminiferal analysis. Mar. Geol. v. 154, 287–304.
Cohen, J.E., Small, C., Mellinger, A., Gallup, J., Sachs, J., 1997. Estimates of coastal populations. Science 278 (1209 LP-1213).
Cohen-Seffer, R., Greenbaum, N., Sivan, D., Jull, T., Barmeir, E., Croitoru, S., Inbar, M., 2005. Late Pleistocene-Holocene marsh episodes along the Carmel coast, Israel. Quat. Int. 140–141, 103–120.
Cronin, T.M., 2012. Rapid sea-level rise. Quat. Sci. Rev. 56, 11–30.
Dalrymple, R.W., Zaitlin, B.A., Boyd, R., 1992. Estuarine facies models: conceptual basis and stratigraphic implications. J. Sed. Pet. 62, 1130–1146.
Duncan, C.S., Goff, J.A., Austin Jr., J.A., C. S. Fulthorpe, C.S., 2000. Tracking the last sea level cycle: seafloor morphology and shallow stratigraphy of the latest Quaternary New Jersey middle continental shelf. Mar. Geol. 170, 395–421.
Farrand, W.R., Ronen, A., 1974. Observations on the kurkar-hamra succession on the Carmel Coastal Plain. Tel Aviv 1, 45–54.
FitzGerald, D.M., Fenster, M.S., Argow, B.A., Buyenevich, I.V., 2008. Coastal impacts due to sea-level rise. Annu. Rev. Earth Planet. Sci. 36, 601–647.
Flannery, K.V., 1973. The origins of agriculture. Annu. Rev. Anthropol. 2, 271–310.
Forman, S.L., Sagintayev, Z., Sultan, M., Smith, S., Becker, R., Kendall, M., Marin, L., 2008. The twentieth-century migration of parabolic dunes and wetland formation at Cape Cod National Sea Shore, Massachusetts, USA: landscape response to a legacy of environmental disturbance. Holocene 18, 765–774.
Frechen, M., Dermann, B., Boenigk, W., Ronen, A., 2001. Luminescence chronology of aeolianites from the section at Givat Olga Coastal Plan of Israel. Quat. Sci. Rev. 20, 805–809.
Galili, E., Weinstein-Evron, M., Hershkovitz, I., Gopher, A., Kislev, M., Lernau, O., Kolska-Horwitz, L., Lernaut, H., 1993. Atlit-Yam: a prehistoric site on the sea floor off the Israeli coast. J. F. Archaeol. 20, 133–157.
Gautney, J.R., Holliday, T.W., 2015. New estimations of habitable land area and human population size at the last glacial maximum. J. Archaeol. Sci. 58, 103–112.
Goff, J.A., Flood, R.D., Austin Jr., J.A., Scwab, W.C., Christensen, B., Browne, C.M., Denny, J.F., Baldwin, W.E., 2015. The impact of Hurricane Sandy on the shoreface and inner shelf of Fire Island, New York: large bedform migration and limited erosion. Cont. Shelf Res. 98, 13–25.
Goodman-Tchernov, B., Katz, O., 2016. Holocene-era submerged notches along the southern Levantine coastline: punctuated sea level rise? Quat. Int. 401, 17–27.
Goodman-Tchernov, B.N., Austin Jr., J.A., 2015. Deterioration of Israel's Caesarea Maritima's ancient harbor linked to repeated tsunami events identified in geophysical mapping of offshore stratigraphy. J. Archaeol. Sci. Rep. 3, 444–454.
Gopher, A., 1993. Sixth-fifth millennia B.C. settlements in the Coastal Plain, Israel. Paléorient 19, 55–63.
Gvirtzman, G., Netster, M., Katsav, E., 1998. Last-glacial to Holocene Kurkar ridges, hamra soils, and dune fields in the coastal belt of central Israel. Isr. J. Earth Sci. 47, 27–46.
Hinrichsen, D., 1996. Coasts in crisis. Issues Sci. Technol. 12, 39–47.
Hole, F., 1984. A Reassessment of the Neolithic Revolutionrr. Paléorient 10, 49–60.
Holum, K., Raban, A., 1996. Caesarea Maritima: a Retrospective After Two Millenium. Brill. 693 pages. Boston, USA.
Jones, R.E., Sarris, A., 2000. Geophysical and related techniques applied to archaeological survey in the Mediterranean: a review. J. Mediterr. Archaeol. 13, 3–75.
Kadosh, D., Sivan, D., Kutiel, H., Weinstein-Evron, M., 2004. A late Quaternary paleoenvironmental sequence from Dor, Carmel coastal plain, Israel. Palynology 28, 143–157.
Lambeck, K., Rouby, H., Purcell, A., Sun, Y., Sambridge, M., 2014. Sea level and global ice volumes from the Last Glacial Maximum to the Holocene. Proc. Natl. Acad. Sci. 111, 15,296–15,303.
Langgut, D., Almogi-Labin, Ak, Bar-Matthews, M., Weinstein-Evron, M., 2011. Vegetation and climate changes in the South Eastern Mediterranean during the Last Glacial-Interglacial cycle (86 ka): new marine pollen record. Quat. Sci. Rev. 30, 3960–3972.
Levy, Y., 1974. Sedimentary reflection of depositional environment in the Bardawil Lagoon, Northern Sinai. J. Sed. Pet. 44, 219–227.
Marriner, N., Flaux, C., Morhange, C., Stanley, J.-D., 2013. Tracking Nile Delta vulnerability to Holocene change. PLoS One 8, e69195. http://dx.doi.org/10.1371/journal.pone.0069195.
Mauz, B., Hijma, M.P., Amorosi, A., Porat, N., Galili, E., Bloemendal, J., 2013. Aeolian beach ridges and their significance for climate and sea level: concept and insight from the Levant coast (East Mediterranean). Earth Sci. Rev. 121, 31–54.
Neev, D., Shachnai, E., Hall, J.K., Bakler, N., Ben Avraham, Z., 1978. The young (post lower Pliocene) geological history of the Caesarea structure. Isr. J. Earth Sci. 27, 43–64.
Nordfjord, S., Goff, J.A., Austin Jr., J.A., Gulick, S.P.S., 2006. Seismic facies of incised valley-fills, New Jersey continental shelf: implications for erosion and preservation processes acting during late Pleistocene/Holocene transgression. J. Sed. Res. 76, 1284–1303.
Parcak, S.H., 2009. Satellite remote sensing for archaeology. Routledge, 285 pages, New York.
Porat, N., Avital, A., Frechen, M., Almogi-Lavin, A., 2003. Chronology of upper Quaternary offshore successsions from the southeastern Mediterranean Sea, Israel. Quat. Sci. Rev. 22, 1191–1199.
Porat, N., Wintle, A.G., Ritte, M., 2004. Mode and timing of kurkar and hamra formation, central coastal plain, Israel. Isr. J. Earth Sci. 53, 13–25.
Putterman, L., 2008. Agriculture, diffusion and development: ripple effects of the Neolithic Revolution. Economica 75, 729–748.
Pye, K., Tsoar, H., 2009. Aeolian Sand and Sand Dunes, Second ed. Springer, Berlin (476 pp.).
Raban, A., 1983. Submerged prehistoric sites off the Mediterranean coast of Israel. In: Quaternary Coastlines and Marine Archaeology. Academic Press, New York, pp. 215–232.

Raban, A., 2009. The Harbour of Sebastos (Caesarea Maritima) in its Roman Mediterranean Context. 1930 BAR International Series, Oxford.
Raban, A., Galili, E., 1985. Recent maritime archaeological research in Israel: a preliminary report. Int. J. Naut. Archaeol. 14, 321–356.
Roskin, J., Sivan, D., Shtienberg, G., Roskin, E., Porat, N., Bookman, R., 2015. Natural and human controls of the Holocene evolution of the beach, aeolian sand and dunes of Caesarea (Israel). Aeolian Res. 19, 65–85.
Sade, A.R., Hall, J.K., Amit, G., Golan, A., Gur-Arieh, L., Tibor, G., 2006. The Israel national bathymetric survey—a new look at the seafloor off Israel. Isr. J. Earth Sci. 55, 185–187.
Sauer, C.O., 1952. Agricultural Origins and Dispersals. MIT Press, Cambridge, MA.
Schattner, U., Lazar, M., Tibor, G., Ben-Avraham, Z., Makovsky, Y., 2010. Filling up the shelf – A sedimentary response to the last post glacial sea rise. Mar. Geol. 278, 165–176.
Shtienberg, G., Zviely, D., Sivan, D., Lazar, M., 2014. Two centuries of coastal change at Caesarea, Israel: natural processes vs. human intervention. Geo-Mar. Lett. 34, 365–379.
Shtienberg, G., Dix, J., Waldmann, N., Makovsky, Y., Golan, A., Sivan, D., 2016. Late-Pleistocene evolution of the continental shelf of central Israel, a case study from Hadera. Geomorph 261, 200–211.
Shtienberg, G., Dix, J., Roskin, J., Waldmann, N., Bookman, R., Bialik, O.M., Porat, N., Taha, N., Sivan, D., 2017. New perspectives on coastal landscape reconstruction during the Late Quaternary: a test case from central Israel. Palaeogeog. Palaeocl. Palaeoecol 468. pp. 503–519.
Sivan, D., Porat, N., 2004. Evidence from luminescence for Late Pleistocene formation of calcareous aeolianite (kurkar) and paleosol (hamra) in the Carmel Coast. Isr. Paleogeogr. Paleoclimatol. Paleoecol. 211, 95–106.
Small, C., Nicholls, R.J., 2003. A global analysis of human settlement in coastal zones. J. Coast. Res. 19, 584.
Stefani, M., Vincenzi, S., 2005. The interplay of eustasy, climate and human activity in the late Quaternary depositional evolution and sedimentary architecture of the Po Delta system. Mar. Geol. 222–223, 19–48.
Tessier, B., Billeaud, I., Sorrel, P., Delsinne, N., Lesueur, P., 2012. Infilling stratigraphy of macrotidal tide-dominated estuaries. controlling mechanisms: Sea-level fluctuations, bedrock morphology, sediment supply and climate changes (The examples of the Seine estuary and Mont-Saint-Michel Bay, English channel, NW France). Sed. Geol. 279, 62–73.
Thorne, J.A., Swift, D.J.P., 1991. Sedimentation on continental margins,VI: a regime model for depositional sequences, their component system tracts, and bounding surfaces. In: Swift, D.J.P. (Ed.), Shelf Sand and Sandstone Bodies: Geometry, Facies and Sequence Stratigraphy, Special Publications of the International Association of Sedimentologists 14. Wiley, Hoboken, New Jersey, pp. 189–255.
Törnqvist, T.E., Bick, S.J., González, J.L., van der Borg, K., de Jong, A.F.M., 2004. Tracking the sea-level signature of the 8.2 ka cooling event: new constraints from the Mississippi Delta. Geophys. Res. Lett. 31, 1–4. http://dx.doi.org/10.1029/2004GL021429.
Tsatskin, A., Ronen, A., 1999. Micromorphology of a Mousterian paleosol in aeolianites at the site Habonim, Israel. Catena 34, 365–384.
Tsoar, H., 2000. Geomorphology and paleogeography of sand dunes that have formed the kurkar ridges in the coastal plain of Israel. Isr. J. Earth Sci. 49, 189–196.
Tyuleneva, N., Braun, Y., Katz, T., Suchkov, I., Goodman-Tchernov, B., 2017. A new chalcolithic-era tsunami event identified in the offshore sedimentary record of Jisr al-Zarka. Mar. Geol, 396, 67–78.
Vella, C., Feury, T.-J., Raccasi, G., Provansal, M., Sabaier, F., Bourcier, M., 2005. Evolution of the Rhone delta plain in the Holocene. Mar. Geol. 222–223, 235–265.
Vitousek, P.M., Mooney, H. a., Lubchenco, J., Melillo, J.M., 1997. Human domination of earth's ecosystems. Science 277, 494–499.
Waelbroeck, C., Labeyri, L., Michel, E., Duplessy, J.C., McManus, J.F., Lambeck, K., Balbon, E., Labracherie, M., 2002. Sea-level and deep water temperature changes derived from benthic foraminifera isotopic records. Quat. Sci. Rev. 21, 295–305.
Weisdorf, J.L., 2005. From foraging to farming: explaining the neolithic revolution. J. Econ. Surv. 19, 561–586. http://dx.doi.org/10.1111/j.0950-0804.2005.00259.x.
Wessel, P., Smith, W.H.F., 1998. New, improved version of the Generic Mapping Tools released. EOS Trans. AGU 79, 579.
White, G.G., King, T.F., 2007. The Archaeological Survey Manual. Left Coast Press, Inc., Walnut Creek.
Woodward, J.C., Macklin, M.G., Krom, M.D., Williams, M.A.J., 2008. The Nile: evolution, quaternary river environments and material fluxes. Large Rivers Geomorphol. Manag. 261–292.
Zviely, D., Sivan, D., Ecker, A., Bakler, N., Rohrlich, V., Galili, E., Boaretto, E., Klein, M., Kit, E., 2006. Holocene evolution of Haifa Bay area, Israel, and it influence on ancient tell settlements. Holocene 15, 849–861.